

Exciton Basis Description of Ultrafast Triplet Separation in Pentacene-(Tetracene)2-Pentacene Intramolecular Singlet Fission Chromophore.

Arifa Nazir,[†] Alok Shukla,[†] and Sumit Mazumdar^{*,‡}

[†]*Department of Physics, Indian Institute of Technology Bombay, Powai, Mumbai 400076, India*

[‡]*Department of Physics, and the Department of Chemistry, University of Arizona, Tucson, AZ 85721, USA*

E-mail: {*}mazumdar@arizona.edu

Abstract

Precise understanding of the electronic structures of optically dark triplet-triplet multiexcitons that are the intermediate states in singlet fission (SF) continues to be a challenge. This is particularly true for intramolecular singlet fission (iSF) chromophores, that are oligomers of large monomer molecules. We have performed quantum many-body calculations of the complete set of excited states relevant to iSF in Pentacene-(Tetracene)2-Pentacene oligomers, consisting of two terminal pentacene monomers linked by two tetracene monomers. Our computations use an exciton basis that gives physical pictorial descriptions of all eigenstates, and are performed over an active space of twenty-eight monomer molecular orbitals, including configuration interaction with all relevant quadruple excitations within the active space, thereby ensuring very high precision. We discuss the many-electron structures of the optical predominantly intramonomer spin-singlets, intermonomer charge-transfer excitations,

and most importantly, the complete set of low energy covalent triplet-triplet multi-excitons. We are able to explain the weak binding energy of the pentacene-tetracene triplet-triplet eigenstate that is generated following photoexcitation. We explain the increase in lifetime with increasing numbers of tetracene monomers of the transient absorption associated with contiguous pentacene-tetracene triplet-triplet in this family of oligomers. We are consequently able to give a pictorial description of the triplet separation following generation of the initial triplet-triplet, leading to a state with individual triplets occupying only the two pentacene monomers. We expect many applications of our theoretical approach to triplet separation.

1 Introduction

The optically dark triplet-triplet biexciton $^1(T_1T_1)$, a bound state of the two lowest triplets T_1 in π -conjugated carbon(C)-based systems, continues to be of strong experimental and theoretical interest. First discussed in the context of linear π -conjugated polyenes, its energetic location below the lowest optically allowed state¹ gave conclusive evidence of strong electron-electron correlations in linear polyenes.²⁻⁴ The latter theoretical results led to more detailed investigations of electron correlation effects in polyacetylene and related π -conjugated polymers.⁵⁻⁸ More recently, the $^1(T_1T_1)$ is receiving intense scrutiny in the context of singlet fission (SF),⁹⁻¹⁵ which refers to the spin-allowed internal conversion of the optical exciton of a multichromophore π -conjugated system into $^1(T_1T_1)$, where the two triplets T_1 occupy distinct chromophore monomers. Should the binding energy E_b between the individual triplets T_1 in the triplet-triplet state $^1(T_1T_1)$ be small, separation into two free triplets, each of which subsequently contributes to charge generation, becomes conceivable. While the possibility of commercial development of organic solar cells with significantly enhanced quantum efficiency has driven much of the current research on SF, additional impetus comes from the realization that the spin-quintet $^5(T_1T_1)$ may be utilized in quantum information devices.¹⁶⁻²¹ There is hence significant effort to reach clear understanding of the dependence

of the nature of the spin entanglement and the lifetime of the $^1(\text{T}_1\text{T}_1)$ on bonding motifs.

While initial research on SF focused on *intermolecular* SF (xSF), in which the two triplets of $^1(\text{T}_1\text{T}_1)$ occupy nonbonded chromophore monomers, interest has subsequently shifted to *intramolecular* SF (iSF), that occurs in longer systems consisting of monomer chromophore molecules linked directly by chemical bonds or by bridge molecules. Current experimental challenge is to design iSF chromophores in which there occurs rapid $^1(\text{T}_1\text{T}_1)$ generation that overcomes other competing photophysical processes, followed by rapid dissociation into free triplets, or at least slow triplet recombination. Meeting both requirements simultaneously is difficult, as rapid $^1(\text{T}_1\text{T}_1)$ generation requires strong intermonomer coupling,^{22,23} which in turn leads to strong E_b that prevents triplet separation and is responsible for triplet recombination. Indeed, both experiments and computations find E_b in the bulk of iSF compounds to be substantial and nonconducive to free triplet generation. Understanding the precise electronic structures of the $^1(\text{T}_1\text{T}_1)$ in different families of iSF chromophores, the relationship between bonding motifs and triplet-triplet binding energy, and in particular, the paths to triplet separation are all essential for reaching optimized procedures for controlled triplet pair formation and decay rates.

In what follows we describe our theoretical approach to understand the photophysics of one family of iSF compounds that has shown great promise towards overcoming the above challenge. In the process of understanding this particular family we develop full many-body methods that can be used to obtain clear quantum mechanical descriptions of ground and excited state absorptions, as well as triplet-triplet binding and separation in large iSF molecules that will be useful for the successful design of future iSF chromophores.

2 Motivation of work

The immediate focus of our theoretical research is to understand the detailed mechanism of triplet-triplet biexciton generation and subsequent unusually efficient triplet separation as ob-

served experimentally in the family of pentacene-(tetracene) $_n$ -pentacene oligomers.²⁴ These compounds consist of pentacene monomers linked by multiple tetracene bridge monomers (see Fig. 1(a)), hereafter **P-T $_n$ -P** (here **P** and **T** represent pentacene and tetracene monomers, respectively, and **n** is the number of tetracenes). We report calculations specifically for **n** = 2. In what follows we will distinguish between triplet-triplet configurations in which triplet excitations occupy only pentacene monomers, $^1(T_{1[P1]}T_{1[P2]})$, and those in which the triplets occupy both pentacene and tetracene monomers. Triplets in pentacene-tetracene triplet-triplets can occupy nearest neighbor monomers or separated more distant monomers. The former will be written as $^1(T_{1[P1]}T_{1[T1]})$, with the understanding that the notation refers to the superposition with the configuration related by spatial symmetry, $^1(T_{1[P2]}T_{1[T2]})$. Similarly second neighbor pentacene-tetracene triplet-triplets will be written as $^1(T_{1[P1]}T_{1[T2]})$, with $^1(T_{1[P2]}T_{1[T1]})$ implied. The authors of the experimental work inferred ultrafast generation of contiguous triplet-triplet pair $^1(T_{1[P1]}T_{1[T1]})$ following photoexcitation of the pentacene singlet optical exciton²⁴ from transient absorption at 1500 nm, an assignment in agreement with earlier theoretical work.²⁵ This excited state absorption (ESA) was shortlived, and within ultrafast times was replaced by triplet absorption in the visible from pentacene alone. According to the authors, the difference in the triplet energies of **T** and **P** monomers (~ 0.4 eV) creates an energy gradient that drives triplet migration and transition to the lowest energy triplet-pair $^1(T_{1[P1]}T_{1[P2]})$. The latter has very long lifetime,²⁴ as triplet-triplet recombination is energetically uphill.

While the experimental results are promising, they raised intriguing theoretical and experimental questions. In the context of **n** = 1, the relevant questions are as follows. First, whether contiguous triplet-triplet $^1(T_{1[P1]}T_{1[T1]})$ and separated triplet-triplet $^1(T_{1[P1]}T_{1[P2]})$ indeed constituted completely distinct eigenstates, in view of the small energy difference of between **T** versus **P** triplets (0.4 eV) relative to the realistic intermonomer hopping integral ($\sim 1.5 - 2.2$ eV) that would be “mixing up” the configurations. Second, whether triplet migration is indeed behind the generation of the separated triplet-pair. The latter question is

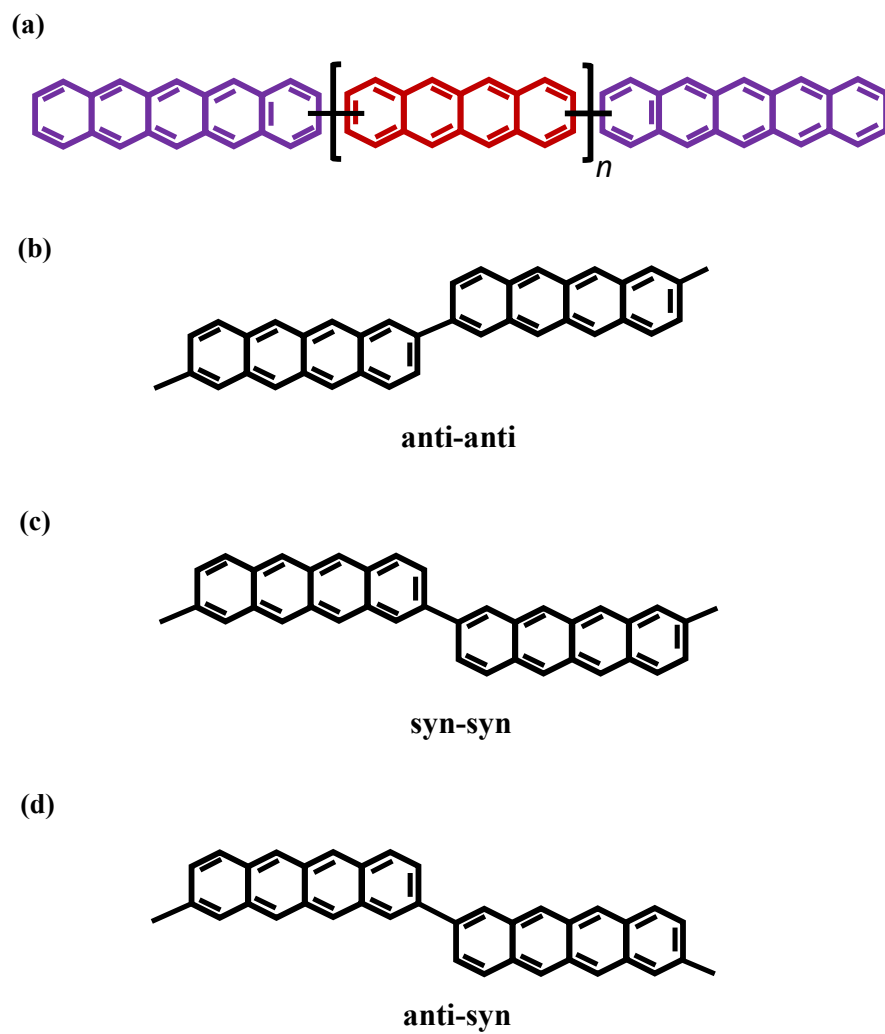


Figure 1: (Color online) (a) Schematic structure of the **P-Tn-P** compounds investigated experimentally.²⁴ (b) *anti-anti* (c) *syn-syn* and (d) *syn-anti* bonding motifs investigated theoretically for the **n=2** molecule.

reasonable, and is based on the earlier demonstration of direct end-to-end (**P** to **P**) CT being the dominant path to $^1(\text{T}_{1[P1]}\text{T}_{1[P2]})$ generation in **P**- β -**P** iSF compounds with β = benzene, naphthalene and anthracene.²⁶ In recent theoretical work on **P-T-P**²⁷ we have shown explicitly that both these assumptions are correct: contiguous triplet-triplet generation followed by triplet migration is indeed the dominant path to separated triplet-pair generation. Direct **P** to **P** CT is the preferred path to iSF only for short bridge molecules with relatively high bridge monomer absorption threshold, and is replaced by nearest neighbor CT when the bridge monomer absorption energy is close to that of the terminal chromophore molecules.

The experimental observations for the $n > 1$ **P-T_n-P** oligomers raise different, though related, questions.

(i) Transient absorption at 1500 nm, associated strictly with the contiguous triplet-triplet²⁵ is also observed in $n = 2$ and $n = 3$. The triplet-triplet binding energy E_b of the **PT** dimer has earlier been calculated to be ~ 0.09 eV,²⁸ significantly larger than thermal energy. Straightforward triplet migration from contiguous triplet-triplet $^1(\text{T}_{1[P1]}\text{T}_{1[T1]})$ to separated triplet-triplet $^1(\text{T}_{1[P1]}\text{T}_{1[T2]})$ requires overcoming E_b and appears unlikely. Note that previous attempt to attain triplet separation in homo-oligomeric polypentacene had failed,²⁹ an experimental result that is in agreement with the large E_b calculated for bipentacene.²⁸ What then is the mechanism through which this binding energy is overcome in $n > 1$ **P-T_n-P** ?

(ii) A second interesting experimental observation is that the the lifetime of the 1500 nm ESA that is used to identify the contiguous triplet-triplet is unresolvably fast in $n = 1$, and is 2.6 ps and 5.7 ps in $n = 2$ and $n = 3$, respectively.²⁴ The increasing lifetimes of the contiguous triplet-triplet in the longer oligomers is not expected within the simplest triplet exciton migration scenario. The increase in lifetimes implies that either the contiguous triplet-triplet lasts longer with increasing n , or that simplest classification of triplet-triplets as contiguous versus separated may require modification. This, in turn, raises the question as to whether distinct pentacene-tetracene and pentacene-pentacene triplet-triplets continue

to persist in $\mathbf{n} > 1$ **P-T \mathbf{n} -P**, or whether there is some configuration mixing.

A final (albeit minor) issue is whether quantum interference (QI) effect, which plays a strong role in the photophysics of **P- β -P** with β = benzene, naphthalene and anthracene²⁶ but which is virtually nonexistent in **P-T-P** with $\mathbf{n} = 1$, plays any role in $\mathbf{n} > 1$ given the tetracene-tetracene linkages.

Resolutions of the above questions necessarily require precise determinations of electronic structures of the complete set of triplet-triplet multiexciton wavefunctions in the $\mathbf{n} > 1$ **P-T \mathbf{n} -P** oligomers. We present here rigorous many-body description of the spin-singlet excited state spectrum of **P-T2-P**, including both the optical singlet and the multiple optically dark triplet-triplet states. We also present computational results of ground and excited state absorptions. As in **P-T-P**,²⁷ the ESA computation provides direct evidence for CT-mediated transition from the optical exciton to the triplet-triplet state generated initially. We show that these $\mathbf{n} = 2$ calculations, taken together with the experimental results give pictorial understanding of triplet separation not just in $\mathbf{n} = 2$, but also in $\mathbf{n} = 3$.

3 Theoretical approach

3.1 Model Hamiltonian and parameterization

Accurate computations of the triplet-triplet biexciton remains outside the scope of first principles approaches for systems containing more than 20 π -electrons.^{30,31} This remains true in spite of recent progress with quantum chemical method development.^{32,33} The most dominant contributions to the $^1(\text{T}_1\text{T}_1)$ eigenstates are two electron-two hole (2e-2h) excitations from the Hartree-Fock (HF) ground state configuration, and its correct description absolutely requires incorporation of configuration interaction (CI) with quadruple 4e-4h excitations. The number of such 4e-4h excitations increases explosively with system size. Computations over restricted active spaces (RAS) that include only the highest occupied and lowest unoccupied molecular orbitals (HOMO and LUMO) of monomers do exist in the literature for small iSF

dimers,^{34,35} but are not expected to meet the accuracy requirement for the wavefunctions in the present case. The Density Matrix Renormalization Group approach is hard to implement for nonperiodic systems, and to the best of our knowledge has only been applied to a relatively small dimeric iSF chromophore, also over the same RAS.³⁶

Our large-scale computations of triplet-triplet multiexcitons in **P-T2-P** are done over an active space of 28 MOs, using the well-tested semiempirical π electron-only Pariser-Parr-Pople (PPP) model Hamiltonian, as in our previous work on the **n=1** oligomer.²⁷ The Hamiltonian is written

$$H = \sum_{\langle ij \rangle, \sigma} t_{ij} (c_{i\sigma}^\dagger c_{j\sigma} + c_{j\sigma}^\dagger c_{i\sigma}) + U \sum_i n_{i\uparrow} n_{i\downarrow} + \frac{1}{2} \sum_{i \neq j} V_{ij} (n_i - 1)(n_j - 1) \quad (1)$$

Here $c_{i\sigma}^\dagger$ creates an electron with spin σ on the p_z orbital of C-atom i , $n_{i\sigma} = c_{i\sigma}^\dagger c_{i\sigma}$ is the number of electrons with spin σ on atom i , and $n_i = \sum_\sigma n_{i\sigma}$ is the total number of electrons on the atom. The symbol $\langle \rangle$ refers to nearest neighbor C-atoms and t_{ij} are the corresponding neighbor electron hopping integrals, U the Coulomb repulsion between two π electrons occupying the p_z orbital of the same C-atom, and V_{ij} is long range Coulomb interaction.

Our calculations are for parameters that are the same as in our calculations for **P-T-P**,²⁷ which in turn were chosen based on fittings of optical singlet and triplet states of tetracene and pentacene monomers.^{37,38} All the intramonomer C-C bond lengths (hopping integrals) are taken to be 1.40 Å (−2.4 eV). We have assumed the molecules to be planar for simplicity, with the interunit bond length 1.46 Å and the corresponding hopping integral −2.2 eV, respectively. Monomer rotation effect can be taken into consideration by reducing the interunit t_{ij} by a multiplicative factor of $\cos\theta$, where θ is the dihedral angle.³⁹ Explicit calculations have confirmed that physical conclusions are not altered substantively by ignoring rotation effects.³⁷ The long range Coulomb interactions were parametrized as $V_{ij} = U/\kappa\sqrt{1 + 0.6117R_{ij}^2}$, where R_{ij} is the distance in Å between C-atoms i and j and κ is

an effective dielectric constant.⁴⁰ The onsite Hubbard repulsion U and the dielectric constant κ are taken to be 7.7 eV and 1.3 based on fitting monomer energetics.^{37,38}

3.2 Diagrammatic exciton basis and computational approach

Physical understanding of triplet migration requires a pictorial description of eigenstates that allows clear distinguishing of 1e-1h versus 2e-2h excitations, as well as intra- versus intermonomer excitations. As for **P-T-P**,²⁷ our calculations are done within the diagrammatic molecular exciton basis.⁴¹ We separate the Hamiltonian into intra- and intermonomer terms ($H = H_{intra} + H_{inter}$) where H_{intra} includes all four monomers, and begin with solving H_{intra} within the Hartree-Fock (HF) approximation to arrive at single-particle basis states.⁴² We retain 8 frontier MOs per **P** monomer (4 bonding and 4 antibonding) and 6 frontier MOs per **T** monomer (3 bonding and 3 antibonding), and perform multiple reference singles and doubles configuration interaction (MRSDCI) calculations⁴ for the complete Hamiltonian of Eq. 1 using the molecular exciton basis to obtain accurate energies and wavefunctions (Supporting Information, hereafter SI, section I). The MRSDCI procedure incorporates the most dominant ne-nh excited configurations (n=1-4) that describe each targeted state. The calculation for each eigenstate is done iteratively, with each iteration consisting of two stages. In the first stage we perform a singles and doubles-CI calculation on a basis space of N_{ref} 1e-1h and 2e-2h configurations that best describe the targeted eigenstate. In the second stage we apply the Hamiltonian ($H_{intra} + H_{inter}$) on the N_{ref} reference configurations. This generates 3e-3h and 4e-4h configurations, of which we retain the most dominant ones to give the larger Hamiltonian matrix of dimension N_{total} . The larger Hamiltonian matrix usually also contains new 1e-1h and 2e-2h excited configurations that were not among the original N_{ref} reference configurations, but that are coupled to the 3e-3h and 4e-4h configurations reached from them. The procedure is repeated with updated N_{ref} configurations to reach a new larger Hamiltonian with updated N_{total} , until the convergence criterion is reached. Ground and the excited eigenstate wave functions are therefore treated on the same footing,

while accounting for their multireference character (see SI Section II). Table S1 in SI gives the dimensions of the MRSDCI matrices that were needed to reach convergences within each symmetry subspace. The present calculations represent the largest correlated-electron calculations of triplet-triplet multiexcitons in any iSF chromophore to date.

4 Ground State Absorption

We calculated the fully correlated ground state wavefunction and wavefunctions of all excited states coupled to the ground state by the dipole operator, for all three oligomers in Figs. 1(b)-1(d). Frequency-dependent optical absorption spectra were obtained from the calculated excited state energies and dipole couplings, using Lorentzians with uniform linewidths of 0.05 eV. The absorption spectra, shown in Fig. 2(a), are to be compared against the experimental spectra in reference.²⁴ The near identical absorption spectra for all three linkages indicates that quantum interference²⁶ is nearly nonexistent.

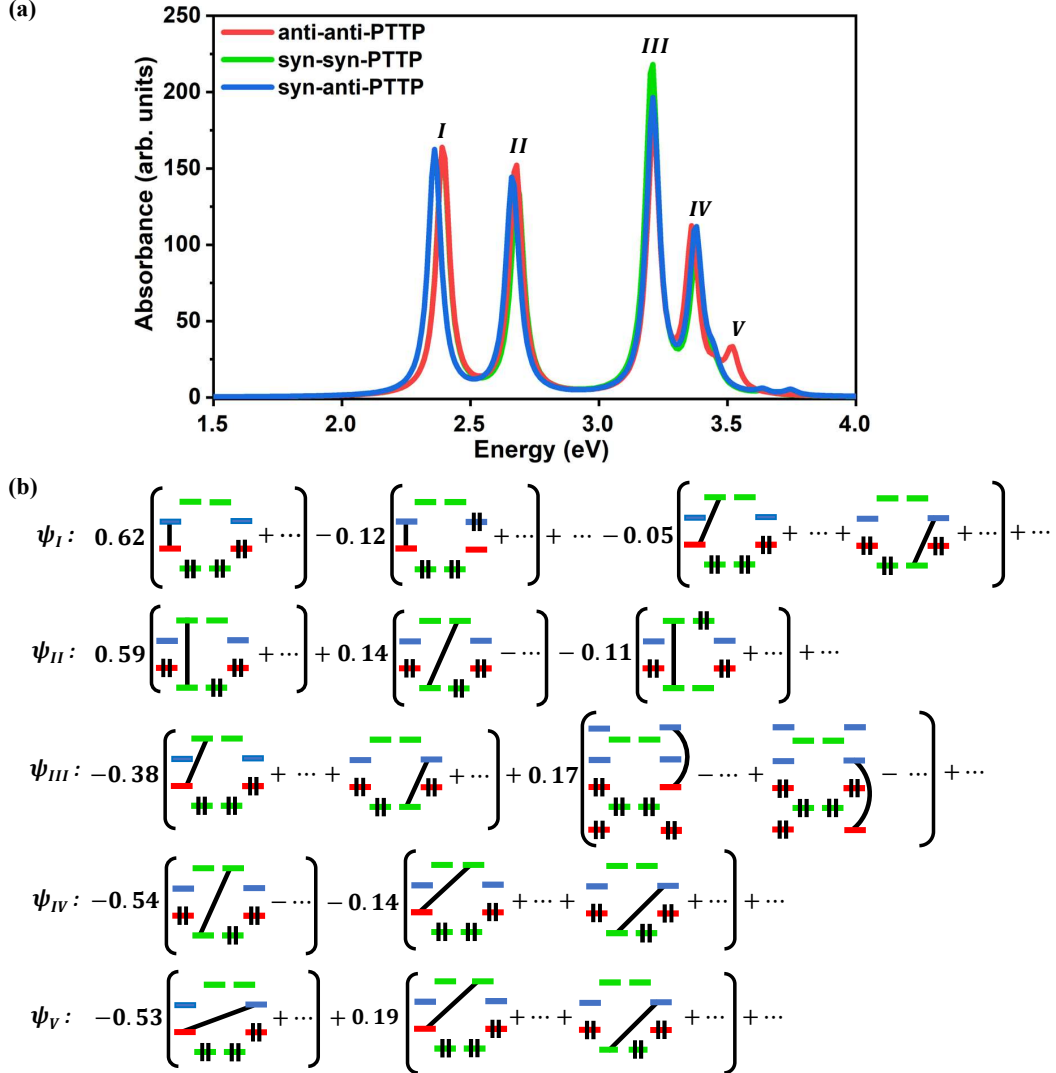


Figure 2: (a) Calculated ground state optical absorption spectra for the anti-anti, syn-syn, and syn-anti configurations of **P-T2-P**. (b) Normalized exciton basis wavefunctions corresponding to the final states of absorptions in anti-anti **P-T2-P**. The outer (inner) pairs of horizontal bars correspond to the highest occupied bonding and lowest unoccupied antibonding MOs (HOMOs and LUMOs) of **P** (**T**). Not shown are lower energy bonding (higher energy antibonding) MOs that are fully occupied (empty). Electron occupancies of MOs are indicated. Lines connecting MOs are spin-singlet bonds. Ellipses correspond to additional configurations related by mirror-plane and charge-conjugation symmetries. See also Figs. S2 and S3 in SI.

Fig. 2(b) shows the most dominant exciton basis components (along with a few select weak components) of the normalized wavefunctions of the final eigenstates corresponding to each absorption band for anti-anti PTTP. The corresponding closely related wavefunctions for syn-syn and syn-anti PTTP are shown in Section III of SI. The final states of the lowest two absorption bands, labeled I and II in Fig. 2(a), are dominated by monomer Frenkel excitons, along with weak **P1**-to-**T1** (and **T2**-to-**P2**) CT components in I and **T1**-to-**T2** CT component in II. Such intermonomer CT are behind the experimentally observed redshifts of the absorptions to optical singlet excitons of iSF oligomers relative to the corresponding monomers,²⁴ and are also drivers of SF (see below). Absorption band III is predominantly due to CT between **P1** and **T1**, with significant mixing with higher energy pentacene intramonomer excitation. The lowest three absorption bands also occur in **P-T-P**, and the final states there are very similar.²⁷ Absorption band IV is predominantly **T1**-to-**T2** CT, with weak but nonzero admixing with second neighbor **P1**-to-**T2** CT. The weak absorption band V is predominantly due to direct long-range CT between **P1** and **P2**. Such long-range CT requires strong constructive quantum interference that can occur only with anti-anti linkage.²⁶

5 CT-mediated $^1(\text{T}_1\text{T}_1)$ generation

Direct evidence for CT-mediated $^1(\text{T}_1\text{T}_1)$ generation in the iSF compounds **P- β -P**, β = benzene, naphthalene and anthracene was seen from the very strong quantum interference effects on the $^1(\text{T}_1\text{T}_1)$ generation time in these. Triple-triplet generation time is significantly faster for anti-linkage than for syn-linkage, and there is one-to-one correspondence between this generation time and the strength of CT absorption, observed both experimentally and computationally.²⁶ As seen in Fig. 2(a), however, interference effect on the absorption spectra are weak here, in that the strengths of absorption bands III and IV are independent of bonding motifs. This is not unexpected, as quantum interference is a consequence of

antiferromagnetic spin correlation driven by the Hubbard U in Eq. (1), but such correlation in effectively one-dimensional systems is short range. The very strong CT absorptions with all three linkages in Fig. 2(a) suggest equally strong role of CT for all linkage motifs. The exciton basis computational approach nevertheless allows demonstration of CT-mediation of $^1(\text{T}_1\text{T}_1)$ generation in **P-T2-P**, as we discuss below.

The authors of a recent experimental work on xSF in pentacene crystals successfully demonstrated CT-mediated $^1(\text{T}_1\text{T}_1)$ generation from careful transient absorption measurements.⁴³ According to the authors CT-mediated SF requires configuration mixing of the singlet Frenkel exciton and CT configuration even in the absence of substantial nuclear rearrangement, which in turn leads to mixing of the CT configuration and the $^1(\text{T}_1\text{T}_1)$ configuration in the dipole-coupled virtual excited state from which the triplet-triplet is generated. In Fig. 3 we have given a schematic representation of the proposed mechanism. The schematic suggests that the eigenstate reached by ESA from Ψ_I in Fig. 2(b) should have weak contribution from a triplet-triplet configuration. In Fig. 4 we have shown the calculated final eigenstates that are reached by ESA from the lowest optical singlet for all three bonding motifs of Fig. 1. In all cases the last many-electron configuration shown is $^1(\text{T}_{1[P1]}\text{T}_{1[T1]})$.

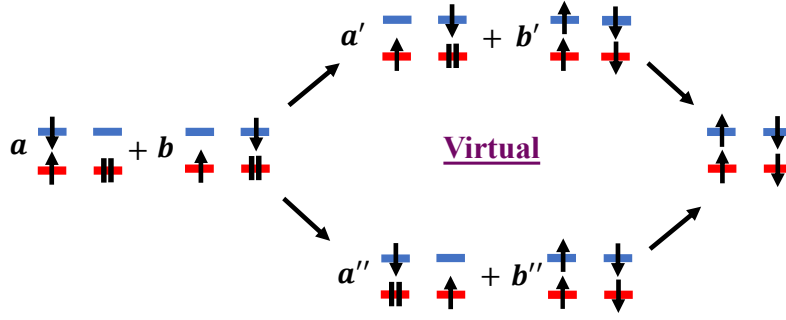


Figure 3: Schematic of CT-mediated SF mechanism in a chromophore dimer. Only the HOMO and LUMO of each monomer and their electronic occupancies are shown. At the very left is the optical singlet, which is a superposition of Frenkel exciton and CT configuration. It is understood that $b \ll a$. Real or virtual optical excitation from this will necessarily lead to the intermediate mixed CT and triplet-triplet state, again with $b' \ll a'$. The final state is the triplet-triplet multiexciton.

$$\begin{aligned}
\text{(a)} \quad & -0.35 \left[\begin{array}{c} \text{---} \text{---} \\ \text{---} \text{---} \\ \text{---} \text{---} \end{array} \right] - \dots + \begin{array}{c} \text{---} \text{---} \\ \text{---} \text{---} \\ \text{---} \text{---} \end{array} + \dots - 0.21 \left[\begin{array}{c} \text{---} \text{---} \\ \text{---} \text{---} \\ \text{---} \text{---} \end{array} \right] + \dots - \begin{array}{c} \text{---} \text{---} \\ \text{---} \text{---} \\ \text{---} \text{---} \end{array} - \dots \\
& + 0.08 \left[\begin{array}{c} \text{---} \text{---} \\ \text{---} \text{---} \\ \text{---} \text{---} \end{array} + \dots + \begin{array}{c} \text{---} \text{---} \\ \text{---} \text{---} \\ \text{---} \text{---} \end{array} + \begin{array}{c} \uparrow \downarrow \\ \uparrow \downarrow \\ \uparrow \downarrow \end{array} - \dots \right] + \dots \\
\text{(b)} \quad & 0.35 \left[\begin{array}{c} \text{---} \text{---} \\ \text{---} \text{---} \\ \text{---} \text{---} \end{array} - \dots - \begin{array}{c} \text{---} \text{---} \\ \text{---} \text{---} \\ \text{---} \text{---} \end{array} - \dots \right] - 0.21 \left[\begin{array}{c} \text{---} \text{---} \\ \text{---} \text{---} \\ \text{---} \text{---} \end{array} \right] + \dots - \begin{array}{c} \text{---} \text{---} \\ \text{---} \text{---} \\ \text{---} \text{---} \end{array} - \dots \\
& + 0.10 \left[\begin{array}{c} \text{---} \text{---} \\ \text{---} \text{---} \\ \text{---} \text{---} \end{array} + \dots \right] - 0.07 \left[\begin{array}{c} \uparrow \downarrow \\ \uparrow \downarrow \\ \uparrow \downarrow \end{array} - \dots \right] + \dots \\
\text{(c)} \quad & 0.51 \left[\begin{array}{c} \text{---} \text{---} \\ \text{---} \text{---} \\ \text{---} \text{---} \end{array} + \begin{array}{c} \text{---} \text{---} \\ \text{---} \text{---} \\ \text{---} \text{---} \end{array} \right] - 0.26 \left[\begin{array}{c} \text{---} \text{---} \\ \text{---} \text{---} \\ \text{---} \text{---} \end{array} - \begin{array}{c} \text{---} \text{---} \\ \text{---} \text{---} \\ \text{---} \text{---} \end{array} \right] \\
& + 0.13 \left[\begin{array}{c} \uparrow \downarrow \\ \uparrow \downarrow \\ \uparrow \downarrow \end{array} + \begin{array}{c} \text{---} \text{---} \\ \text{---} \text{---} \\ \text{---} \text{---} \end{array} \right] - 0.11 \left[\begin{array}{c} \uparrow \downarrow \\ \uparrow \downarrow \\ \uparrow \downarrow \end{array} \right] + \dots
\end{aligned}$$

Figure 4: Normalized wavefunctions of eigenstates to which ESAs from the optical spin singlet state are the strongest, for (a) anti-anti, (b) syn-syn, and (c) syn-anti connectivity. In agreement with the schematic of Fig. 3(b) in each case the eigenstate has a weak but nonvanishing ${}^1(T_{1[P1]}T_{1[T1]})$ component.

6 Triplet-Triplet States.

6.1 Wavefunctions and Energies.

In Fig. 5 we show the dominant exciton basis configurations that constitute the four distinct classes of triplet-triplet eigenstates in anti-anti **P-T2-P**. We emphasize that our near-exact wavefunctions show no mixing between pentacene-pentacene and pentacene-tetracene triplet-triplet configurations, or between the latter and tetracene-tetracene triplet-triplet. Table 1 gives the corresponding calculated energies, to be compared against the calculated energy of 2.39 eV of the lowest singlet exciton (Ψ_I in Fig. 2(a)). The corresponding data for syn-syn and syn-anti bonding motifs are given in sections VI-VIII of SI. The lowest energy eigenstate with triplets localized on the terminal pentacene monomers is nearly identical to that in **P-T-P**, while the highest energy eigenstate with triplets localized on tetracenes is absent there. More interesting are the pairs of doubly degenerate triplet-triplets occupying pentacene and tetracene monomers, shown in Figs. 5(b) and (c). These wavefunctions are not simply contiguous or separated triplet-triplets, but their superpositions. We have labeled the pair of states with larger contribution from neighboring monomers as $^1(T_{1[P1]}T_{1[T1][T2]})$ and the pair of states with larger contribution from second neighbor monomers as $^1(T_{1[P1]}T_{1[T2][T1]})$, respectively. The similar natures of the superpositions of the triplet-triplet configurations in Figs. 5(b) and (c) explains the very small energy difference between the corresponding eigenstates (Table I), which is nearly an order of magnitude smaller than the previously calculated binding energy of ~ 0.09 eV of the pentacene-tetracene dimer triplet-triplet²⁸ as well as thermal energy.

6.2 Excited State Absorptions from pentacene-tetracene triplet-triplets

The significant contributions by the contiguous pentacene-tetracene triplet-triplet $^1(T_{1[P1]}T_{1[T1]})$ to both pairs of triplet-triplet eigenstates (b) and (c) suggest that both will exhibit ESA to

$$\begin{aligned}
\text{(a)} \quad {}^1(T_{1[P1]}T_{1[P2]}) &= 0.86 \left[\begin{array}{c} \uparrow \downarrow \\ \uparrow \downarrow \\ \uparrow \downarrow \end{array} \right] - 0.18 \left[\begin{array}{c} \uparrow \downarrow \\ \uparrow \downarrow \\ \uparrow \downarrow \end{array} \right] + \dots \\
\text{(b)} \quad {}^1(T_{1[P1]}T_{1[T1][T2]}) &= 0.51 \left[\begin{array}{c} \uparrow \downarrow \\ \uparrow \downarrow \\ \uparrow \downarrow \end{array} \right] \pm \dots - 0.34 \left[\begin{array}{c} \uparrow \downarrow \\ \uparrow \downarrow \\ \uparrow \downarrow \end{array} \right] \pm \dots + \dots \\
\text{(c)} \quad {}^1(T_{1[P1]}T_{1[T2][T1]}) &= -0.51 \left[\begin{array}{c} \uparrow \downarrow \\ \uparrow \downarrow \\ \uparrow \downarrow \end{array} \right] \pm \dots - 0.34 \left[\begin{array}{c} \uparrow \downarrow \\ \uparrow \downarrow \\ \uparrow \downarrow \end{array} \right] \pm \dots + \dots \\
\text{(d)} \quad {}^1(T_{1[T1]}T_{1[T2]}) &= -0.84 \left[\begin{array}{c} \uparrow \downarrow \\ \uparrow \downarrow \\ \uparrow \downarrow \end{array} \right] + 0.16 \left[\begin{array}{c} \uparrow \downarrow \\ \uparrow \downarrow \\ \uparrow \downarrow \end{array} \right] + \dots + \dots
\end{aligned}$$

Figure 5: Dominant components of normalized triplet-triplet eigenstates of anti-anti **P-T2-P** (a) ${}^1(T_{1[P1]}T_{1[P2]})$; (b) ${}^1(T_{1[P1]}T_{1[T1][T2]})$, superposition of ${}^1(T_{1[P1]}T_{1[T1]})$ and ${}^1(T_{1[P1]}T_{1[T2]})$; (c) ${}^1(T_{1[P1]}T_{1[T2][T1]})$, also a superposition of the same basic triplet-triplet configurations as in (b) but with the relative weights reversed; and (d) ${}^1(T_{1[T1]}T_{1[T2]})$ states in anti-anti **P-T2-P**. Eigenstates (b) and (c) are each doubly degenerate.

Table 1: Calculated energies (in eV) for ${}^1(T_{1[P1]}T_{1[P2]})$, ${}^1(T_{1[P1]}T_{1[T1][T2]})$, ${}^1(T_{1[P1]}T_{1[T2][T1]})$ and ${}^1(T_{1[T1]}T_{1[T2]})$ for anti-anti **P-T2-P**. The calculated energy of pentacene singlet exciton is 2.39 eV.

State	Energy (eV)
${}^1(T_{1[P1]}T_{1[P2]})$	2.09
${}^1(T_{1[P1]}T_{1[T1][T2]})$	2.48
${}^1(T_{1[P1]}T_{1[T2][T1]})$	2.49
${}^1(T_{1[T1]}T_{1[T2]})$	2.77

the same singlet CT state,²⁵ albeit with weaker intensity from states (c) with lower relative weight of the contiguous triplet-triplet. We have calculated ESAs from both classes of eigenstates. The calculated spectra are shown in Fig. 6. In agreement with previous calculations on pentacene dimers,²⁵ the final state of the calculated ESA at ~ 1698 nm from both triplet-triplets is the same CT state Ψ_{III} in Fig. 2(b). We also find a second weaker ESA to an intramonomer excited eigenstates at a slightly shorter wavelength. A broad band at ~ 1250 nm is indeed visible in the experimental transition absorption spectrum (see Fig. 8 in Supplementary Material of reference²⁴), although it was not identified as a distinct transient absorption by the experimentalists.

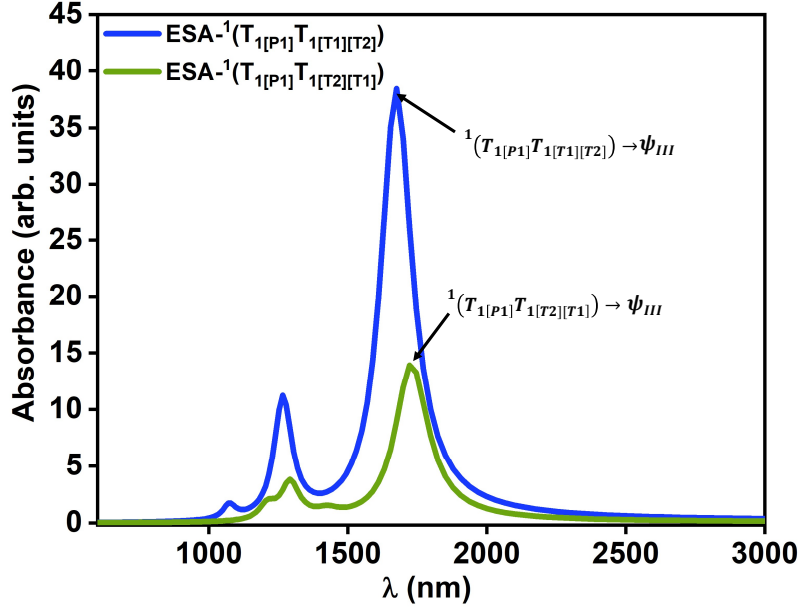


Figure 6: (a) Calculated excited state absorption spectra from the triplet-triplets $^1(T_{1[P1]}T_{1[T1][T2]})$ and $^1(T_{1[P1]}T_{1[T2][T1]})$ for the anti-anti configuration of **P-T2-P**.

7 Discussion and Conclusion

In summary, we have performed high level configuration interaction calculations of the electronic structures of optically allowed singlet and optically dark triplet-triplet eigenstates of **P-T2-P**. We have also performed calculations of ground and excited state absorption

spectra, and have obtained in both cases pictorial descriptions of the final eigenstates to which these absorptions occur, in order to understand why the “cleft” mechanism²⁴ allows generation of weakly bound triplet-triplets with very long lifetimes. In Fig. 7 we present a schematic of the mechanism of initial pentacene-tetracene triplet-triplet generation and separation, followed by the final generation of the pentacene-pentacene triplet-triplet.

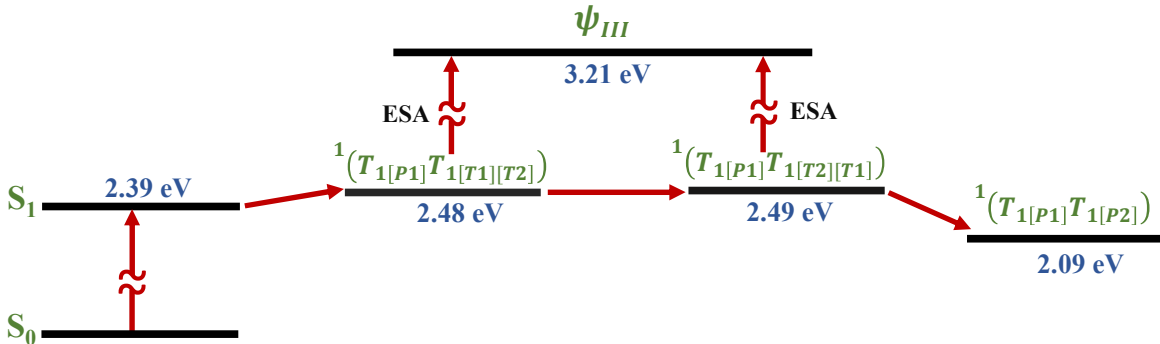


Figure 7: Schematic of the mechanism of triplet-triplet generation and separation in **P-T2-P** (see text).

As in the case of **P-T-P**, we found that pentacene-tetracene and pentacene-pentacene triplet-triplets constitute distinct eigenstates, in spite of the intermolecular electron hopping integral being significantly larger than the difference between tetracene and pentacene triplet energies. The significantly lower energy of $^1(T_{1[P1]}T_{1[P2]})$ confers long lifetime to this state, as recombination would be forbiddingly uphill. More importantly though, this energy gradient leading to the final triplet-triplet eigenstate influences the composition of the intermediate pentacene-tetracene triplet-triplet eigenstates in **P-T2-P**; these can no longer be classified as contiguous versus separated. Doubly degenerate pairs of pentacene-tetracene triplet-triplet eigenstates are each quantum mechanical superpositions of configurations with triplets occupying nearest neighbor monomers as well as second neighbor monomers. The eigenstates with larger relative weight of the configurations with increased triplet-triplet distance occur at a very slightly higher energy that is thermally accessible. Triplet-triplet binding energy is thus insignificant.

We also reached precise understanding of the increase with increasing \mathbf{n} of the apparent lifetimes of the “contiguous” pentacene-tetracene triplet-triplet, as obtained from the duration of the transient absorption in the IR.²⁴ As shown from computations in Fig. 6 and is indicated in the schematic of Fig. 7, this transient absorption due to CT between neighboring triplets²⁵ will continue to occur even as triplet separation proceeds. There are overall four pentacene-tetracene triplet-triplet eigenstates after taking into consideration spatial symmetries in $\mathbf{n} = 2$. It is to be anticipated that there will be nine such pentacene-tetracene triplet-triplet eigenstates with different relative weights of configurations with contiguous triplets in $\mathbf{n} = 3$. The larger number of such eigenstates ensures greater width of their energy eigenspectrum, and hence longer duration of the near IR transient absorption to the $\mathbf{n} = 3$ equivalent of Ψ_I in Fig. 2(b), as is observed experimentally.

In conclusion, high order CI calculations within the PPP Hamiltonian using the exciton basis not only allow understanding the electronic structures of triplet-triplet excitations, but with creative implementation they will allow understanding in detail photophysical processes that lead to their unbinding. Fast generation of the initial triplet-triplet will continue to be one central goal of SF research, and it is likely that this will lead to even greater focus on iSF (as opposed to xSF) chromophores, precisely systems in which triplet-triplet binding energy is relatively large. Clear understanding of the dependence of charge-transfer and/or triplet exciton migration on bonding motifs then becomes imperative. It is for instance conceivable that bridge monomers with the lowest absorption polarized along the lengths of the molecules, as opposed to transverse to their lengths as is true for acene bridges, will lead to more efficient charge-transfer. This can often be achieved with substitution of carbon atoms with heteroatoms containing lone-pairs of electrons. Greater charge-transfer can conceivably be achieved also by increasing the effective dimensionality of the experimental system. Effective PPP-CI calculations can guide focused experimental search for the “ideal” iSF chromophores. We anticipate many future applications of our theoretical approach.

Supporting Information Available

A detailed description of MRSDCI methodology employed in this work, along with the normalized exciton basis wavefunctions corresponding to the final states of absorptions and triplet-triplet states in syn-syn and syn-anti PT2P, is provided in the Supporting Information.

Acknowledgement

A. S. and S. M. acknowledge fruitful discussions with L. M. Campos (Columbia University) and M. Sfeir (CUNY). Work at University of Arizona Tucson was partially supported by NSF Grant No. NSF-DMR-2301372. Some of the calculations were performed using high performance computing resources maintained by the University of Arizona Research Technologies department and supported by the University of Arizona Technology and Research Initiative Fund, University Information Technology Services, and Research, Innovation, and Impact.

References

- (1) Hudson, B. S.; Kohler, B. E. Linear Polyene Electronic Structure and Spectroscopy. Ann. Rev. Phys. Chem. **1974**, 25, 437–460.
- (2) Schulten, K.; Ohmine, I.; Karplus, M. Correlations effects in the spectra of polyenes. J. Chem. Phys. **1976**, 64, 4422–4441.
- (3) Ramasesha, S.; Soos, Z. G. CORRELATED STATES IN LINEAR POLYENES, RADICALS, AND IONS - EXACT PPP TRANSITION MOMENTS AND SPIN-DENSITIES. J. Chem. Phys. **1984**, 80, 3278–3287.

- (4) Tavan, P.; Schulten, K. Electronic Excitations in Finite and Infinite Polyenes. Phys. Rev. B **1987**, 36, 4337–4358.
- (5) Baeriswyl, D.; Campbell, D. K.; Mazumdar, S. In Conjugated Conducting Polymers; Kiess, H., Ed.; Springer Verlag: Berlin, 1992.
- (6) Soos, Z. G.; Galvao, D. S.; Etemad, S. Fluorescence and excited-state structure of conjugated polymers. Adv. Mater. **1994**, 6, 280–287.
- (7) Ramasesha, S.; Pati, S. K.; Shuai, Z.; Brédas, J. The density matrix renormalization group method: Application to the low-lying electronic states in conjugated polymers. Adv. Quant. Chem. **2000**, 121 – 215.
- (8) Barford, W. Electronic and Optical Properties of Conjugated Polymers; Oxford Science Publications, 2005.
- (9) Smith, M. B.; Michl, J. Recent Advances in Singlet Fission. Annu. Rev. Phys. Chem. **2013**, 64, 361–386.
- (10) Lee, J.; Jadhav, P.; Reuswig, P. D.; Yost, S. R.; Thompson, N. J.; Congreve, D. N.; Hontz, E.; Voorhis, T. V.; Baldo, M. A. Singlet Exciton Fission Photovoltaics. Acc. Chem. Res. **2013**, 46, 1300–1311.
- (11) Rao, A.; Friend, R. H. Harnessing singlet exciton fission to break the Shockley-Queisser limit. Nature Reviews **2017**, 2, 17063.
- (12) Xia, J.; Sanders, S. N.; Cheng, W.; Low, J. Z.; Liu, J.; Campos, L. M.; Sun, T. Singlet fission: Progress and prospects in solar cells. Adv. Mater. **2017**, 29, 1601652.
- (13) Felter, K. M.; Grozema, F. C. Singlet Fission in Crystalline Organic Materials: Recent Insights and Future Directions. J. Phys. Chem. Lett. **2019**, 10, 7208–7214.

- (14) Casillas, R.; Papadopoulos, I.; Ullrich, T.; Thiel, D.; Kunzmann, A.; Guldi, D. M. Molecular insights and concepts to engineer singlet fission energy conversion devices. Energy & Environmental Science **2020**, 13, 2741–2804.
- (15) Baldacchino, A. J.; Collins, M. I.; Nielsen, M. P.; Schmidt, T. W.; McCamey, D. R.; Tayebjee, M. J. Y. Singlet fission photovoltaics: Progress and promising pathways. Chem. Phys. Rev. **2022**, 3, 021304.
- (16) Weiss, L. R.; Bayliss, S. L.; Krafft, F.; Thorley, K. J.; Anthony, J. E.; Bittl, R.; Friend, R. H.; Rao, A.; Greenham, N. C.; Behrends, J. Strongly exchange-coupled triplet pairs in an organic semiconductor. Nat. Phys. **2017**, 13, 176–181.
- (17) Tayebjee, M. J. Y.; Sanders, S. N.; Kumaraswamy, E.; Campos, L. M.; Sfeir, M. Y.; McCamey, D. R. Quintet multiexciton dynamics in singlet fission. Nat. Phys. **2017**, 13, 182–188.
- (18) Smyser, K. E.; Eaves, J. D. Singlet fission for quantum information and quantum computing: the parallel JDE model. Sci. Rep. **2020**, 10, 18480.
- (19) Jacobberger, R. M.; Qiu, Y.; Williams, M. L.; Krzyaniak, M.; Wasielewski, M. R. Using molecular design to enhance the coherence time of quintet multiexcitons generated by singlet fission in single crystals. J. Am. Chem. Soc. **2022**, 144, 2276–2283.
- (20) Dill, R. D.; Smyser, K. E. ; Rugg, B. K.; Damrauer, N. H.; Eaves, J. D. Entangled spin-polarized excitons from singlet fission in a rigid dimer. Nat. Commun. **2023**, 14, 1180.
- (21) A.Yamauchi,; Tanaka1, K.; Fuki, M.; et al., S. F. Room-temperature quantum coherence of entangled multiexcitons in a metal-organic framework. Sci. Adv. **2024**, 10, eadi3147.

- (22) Pensack, R. D.; Tilley, A. J.; Grieco, C.; Purdum, G. E.; Ostroumov, E. E.; Granger, D. B.; Oblinsky, D. G.; Dean, J. C.; Doucette, G. S.; Asbury, J. B.; Loo, Y.-L.; Seferos, D. S.; Anthony, J. E.; Scholes, G. D. Striking the right balance of intermolecular coupling for high-efficiency singlet fission. Chem. Sci. **2018**, 9, 6240–6259.
- (23) Masoomi-Godarzi, S.; Hall, C. R.; Zhang, B.; Gregory, M. A.; White, J. M.; Wong, W. W. H.; Ghiggino, K. P.; Smith, T. A.; Jones, D. A. Competitive Triplet Formation and Recombination in Crystalline Films of Perylenediimide Derivatives: Implications for Singlet Fission. J. Phys. Chem. C **2020**, 124, 11574.
- (24) Pun, A. B.; Asadpoordarvish, A.; Kumarasamy, E.; Tayebjee, M. J. Y.; Niesner, D.; McCamey, D. R.; Sanders, S. N.; Campos, L. M.; Sfeir, M. Y. Ultra-fast intramolecular singlet fission to persistent multiexcitons by molecular design. Nat. Chem. **2019**, 11, 821–828.
- (25) Khan, S.; Mazumdar, S. Theory of Transient Excited State Absorptions in Pentacene and Derivatives: Triplet-Triplet Biexciton versus Free Triplets. J. Phys. Chem. Lett. **2017**, 8, 5943–5948.
- (26) Parenti, K.; Chesler, R.; He, G.; Bhattacharyya, P.; Xiao, B.; Malinowski, D.; Zhang, J.; Yin, X.; Shukla, A.; Mazumdar, S.; Sfeir, M.; Campos, L. The Role of Quantum Interference in Intramolecular Singlet Fission. Nat. Chem. **2023**, 15, 339–346.
- (27) Chesler, R.; Bhattacharyya, P.; Shukla, A.; Mazumdar, S. Distinct contiguous versus separated triplet-pair multiexcitons in an intramolecular singlet fission chromophore. Phys. Rev. B **2024**, 110, L121104.
- (28) Chesler, R.; Khan, S.; Mazumdar, S. Wave Function Based Analysis of Dynamics versus Yield of Free Triplets in Intramolecular Singlet Fission. J. Phys. Chem. A **2020**, 124, 10091–10099.

- (29) Sanders, S. N.; Kumarasamy, E.; Pun, A. B.; Steigerwald, M. L.; Sfeir, M. Y.; Campos, L. M. Singlet Fission in Polypentacene. Chem **2016**, 1, 505–511.
- (30) Kim, H.; Zimmerman, P. M. Coupled double triplet state in singlet fission. Physical Chemistry Chemical Physics **2018**, 20, 30083–30094.
- (31) Rishi, V.; Ravi, M.; Perera, A.; Bartlett, R. J. Dark Doubly Excited States with Modified Coupled Cluster Models: A Reliable Compromise between Cost and Accuracy? J.Phys. Chem. A **2023**, 127, 828–834.
- (32) Shao, Y.; Gan, Z.; Epifanovsky, E.; Gilbert, A. T. B., et al. Advances in molecular quantum chemistry contained in the Q-Chem 4 program package. Mol. Phys. **2015**, 113, 184–215.
- (33) Epifanovsky, E.; Gilbert, A. T. B.; Feng, X.; Lee, J., et al. Software for the frontiers of quantum chemistry: An overview of developments in the Q-Chem 5 package. J. Chem. Phys. **2021**, 155, 084801.
- (34) Korovina, N. V.; Das, S.; Nett, Z.; Feng, X.; Joy, J.; Haiges, R.; Krylov, A. I.; Bradforth, S. E.; Thompson, M. E. Singlet Fission in a Covalently Linked Cofacial Alkynyl-tetracene Dimer. J. Am. Chem. Soc. **2016**, 138, 617–627.
- (35) Korovina, N. V.; Joy, J.; Feng, X. T.; Feltenberger, C.; Krylov, A. I.; Bradforth, S. E.; Thompson, M. E. Linker-Dependent Singlet Fission in Tetracene Dimers. J. Am. Chem. Soc. **2018**, 140, 10179–10190.
- (36) Taffet, E. J.; Beljonne, D.; Scholes, G. Overlap-driven splitting of triplet pairs in singlet fission. J. Am. Chem. Soc. **2020**, 142, 20040–20047.
- (37) Khan, S.; Mazumdar, S. Diagrammatic Exciton Basis Theory of the Photophysics of Pentacene Dimers. J. Phys. Chem. Lett. **2017**, 8, 4468–4478.

- (38) Khan, S.; Mazumdar, S. Optical probes of the quantum-entangled triplet-triplet state in a heteroacene dimer. Phys. Rev. B **2018**, 98, 165202.
- (39) Ramasesha, S.; Albert, I. Sudden polarization in interacting model π -systems: An exact study. Chem. Phys. **1990**, 142, 395 – 402.
- (40) Chandross, M.; Mazumdar, S. Coulomb interactions and linear, nonlinear, and triplet absorption in poly(para-phenylenevinylene). Phys. Rev. B **1997**, 55, 1497–1504.
- (41) Chandross, M.; Shimoi, Y.; Mazumdar, S. Diagrammatic exciton-basis valence-bond theory of linear polyenes. Phys. Rev. B **1999**, 59, 4822–4838.
- (42) Sony, P.; Shukla, A. A general purpose Fortran 90 electronic structure program for conjugated systems using Pariser–Parr–Pople model. Computer Physics Communications **2010**, 181, 821–830.
- (43) Neef, A.; Beaulieu, S.; Hammer, S.; Maklar, J.; Pincelli, T., et al. Orbital-resolved observation of singlet fission. Nature **2023**, 616, 275–279.

Exciton Basis Description of Ultrafast Triplet Separation in Pentacene-(Tetracene)2-Pentacene Intramolecular Singlet Fission Chromophore.

Arifa Nazir¹, Alok Shukla¹, and Sumit Mazumdar²

¹*Department of Physics, Indian Institute of Technology Bombay, Powai, Mumbai 400076, India and*

²*Department of Physics and the Department of Chemistry,*

University of Arizona, Tucson, AZ 85721, USA

I. MOLECULAR EXCITON BASIS AND ACTIVE SPACE

Our objective is to develop intuitive, visual representations of eigenstates. This requires differentiating excitations that remain localized within individual monomers from those that spread over multiple units. To achieve this, we express the PPP Hamiltonian as $H = H_{intra} + H_{inter}$, where it is decomposed into two components:

1. Intra-unit interaction: $H_{intra} = \sum_{\mu} H_{intra}^{\mu}$ represents the sum of PPP Hamiltonians for each molecular unit μ (which includes the two pentacene monomers and two tetracene bridge molecules)
2. Inter-unit interactions: $H_{inter} = \frac{1}{2} \sum_{\nu \neq \mu} H_{inter}^{\nu\mu}$ accounts for hopping (t_{ij}) and Coulomb interactions (V_{ij}) between carbon atoms i and j in different molecular units.

The calculations proceed in multiple steps. First, the intra-unit Hamiltonians (H_{intra}^{μ}) are solved at the Hartree-Fock (HF) level to generate molecular orbitals (MOs) localized on each unit. The configuration interaction (CI) matrix is then constructed by iteratively applying $H = H_{intra} + H_{inter}$ to the most probable configurations that contribute to a given excited state. These configurations, spanning 1e-1h to 4e-4h excitations from the HF ground state, include both neutral states, where the number of π -electrons matches the carbon atom count in each unit, and ionic states, where the units acquire opposite positive and negative charges.

In our MRSDCI calculations, we concentrate on a strategically chosen subset of molecular orbitals (MOs) centered around the chemical potential rather than employing the complete orbital set. To simplify the configuration interaction process, we "freeze" the lowest-energy

bonding MOs, meaning that we do not allow excitations from these orbitals - and we also remove the highest-energy orbitals, which are related to them by charge-conjugation symmetry, from the active space. Consequently, our calculations are performed using active spaces of 28 MOs, divided into 14 bonding and an equal number of antibonding orbitals as shown in Fig. S1. Notably, these represent the largest active spaces ever utilized for $|\text{TT}\rangle$ state calculations.

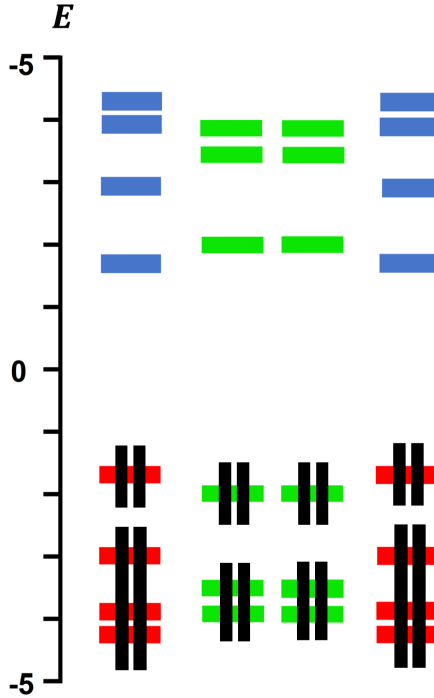


Figure S1. The energy level diagram for P-T-T-P, as determined at the Hartree-Fock (HF) level, shows a total of 28 molecular orbitals (MOs) in active space. The bonding MOs of pentacene are depicted in red, the antibonding MOs in blue, and the MOs of tetracene in green. Electron occupancy is indicated by vertical black lines. Every bonding MO is completely occupied in the HF ground state, whereas every antibonding MO is unoccupied.

II. MULTIREFERENCE SINGLES AND DOUBLES CI

To accurately compute ${}^m(\text{T}_1\text{T}_1)$ energies and wavefunctions, we implement an MRSDCI framework that individually targets each eigenstate. In our approach, configuration interaction (CI) is performed with excitations up to quadruple order starting from the Hartree-Fock

(HF) ground state. Unlike conventional QCI, which exhaustively includes all quadruple excitations, we selectively incorporate only the most relevant n -electron n -hole ($n=1$ to 4) excitations that significantly contribute to each eigenstate. For each eigenstate, the process starts with a comprehensive singles and doubles-CI calculation that spans all the single and double excitations, now including the effects of H_{inter} (i.e., $H_{inter} \neq 0$). During this step, we discard any single and double excitations whose contributions fall below a certain threshold. The remaining configurations form our initial reference set, denoted as N_{ref} . Next, we perform further CI calculations by including additional double excitations derived from the N_{ref} configurations. This step effectively brings in the most important triple and quadruple excitations. These higher-order excitations can interact strongly with new single and double excitations that were not part of the original reference set. By iteratively updating N_{ref} to include these newly significant configurations, we ensure that all dominant excitations: single, double, triple, and quadruple with coefficients of 0.1 or greater are incorporated for each targeted eigenstate. The resulting Hamiltonian, incorporating all these contributions has a total size of N_{total} . Table S1 summarizes the values of N_{total} and N_{ref} for various eigenstates computed with this method.

Table S1. N_{ref} and N_{total} obtained from MRSDCI calculation in *anti-anti*, *syn-syn* and *syn-anti*
PT2P

	anti-anti		syn-syn		syn-anti	
states	N_{ref}	N_{total}	N_{ref}	N_{total}	N_{ref}	N_{total}
S_0S_1	53	2588877	59	3065121	70	3564528
gs CT						
ESA CT	65	3299157	87	4771823	82	4388608
$^1(T_1T_1)$	53	2588877	59	3065121	70	3564528

III. EIGENSTATES THAT CONTRIBUTE TO GROUND-STATE ABSORPTION.

$$\begin{aligned}
\psi_I: & 0.62 \left(\begin{array}{c} \text{---} \quad \text{---} \\ | \quad | \\ \text{---} \quad \text{---} \\ \text{---} \quad \text{---} \end{array} + \dots \right) - 0.12 \left(\begin{array}{c} \text{---} \quad \text{---} \\ | \quad | \\ \text{---} \quad \text{---} \\ \text{---} \quad \text{---} \end{array} + \dots \right) + \dots \\
\psi_{II}: & 0.59 \left(\begin{array}{c} \text{---} \quad \text{---} \\ | \quad | \\ \text{---} \quad \text{---} \\ \text{---} \quad \text{---} \end{array} - \dots \right) + 0.14 \left(\begin{array}{c} \text{---} \quad \text{---} \\ | \quad | \\ \text{---} \quad \text{---} \\ \text{---} \quad \text{---} \end{array} - \dots \right) - 0.11 \left(\begin{array}{c} \text{---} \quad \text{---} \\ | \quad | \\ \text{---} \quad \text{---} \\ \text{---} \quad \text{---} \end{array} - \dots \right) + \dots \\
\psi_{III}: & 0.38 \left(\begin{array}{c} \text{---} \quad \text{---} \\ | \quad | \\ \text{---} \quad \text{---} \\ \text{---} \quad \text{---} \end{array} + \dots + \begin{array}{c} \text{---} \quad \text{---} \\ | \quad | \\ \text{---} \quad \text{---} \\ \text{---} \quad \text{---} \end{array} + \dots \right) - 0.17 \left(\begin{array}{c} \text{---} \quad \text{---} \\ | \quad | \\ \text{---} \quad \text{---} \\ \text{---} \quad \text{---} \end{array} + \dots + \begin{array}{c} \text{---} \quad \text{---} \\ | \quad | \\ \text{---} \quad \text{---} \\ \text{---} \quad \text{---} \end{array} + \dots \right) + \dots \\
\psi_{IV}: & 0.54 \left(\begin{array}{c} \text{---} \quad \text{---} \\ | \quad | \\ \text{---} \quad \text{---} \\ \text{---} \quad \text{---} \end{array} - \dots \right) + 0.14 \left(\begin{array}{c} \text{---} \quad \text{---} \\ | \quad | \\ \text{---} \quad \text{---} \\ \text{---} \quad \text{---} \end{array} - \dots \right) - 0.11 \left(\begin{array}{c} \text{---} \quad \text{---} \\ | \quad | \\ \text{---} \quad \text{---} \\ \text{---} \quad \text{---} \end{array} + \dots + \begin{array}{c} \text{---} \quad \text{---} \\ | \quad | \\ \text{---} \quad \text{---} \\ \text{---} \quad \text{---} \end{array} + \dots \right) + \dots \\
\psi_V: & 0.53 \left(\begin{array}{c} \text{---} \quad \text{---} \\ | \quad | \\ \text{---} \quad \text{---} \\ \text{---} \quad \text{---} \end{array} + \dots \right) - 0.17 \left(\begin{array}{c} \text{---} \quad \text{---} \\ | \quad | \\ \text{---} \quad \text{---} \\ \text{---} \quad \text{---} \end{array} - \dots \right) + 0.16 \left(\begin{array}{c} \text{---} \quad \text{---} \\ | \quad | \\ \text{---} \quad \text{---} \\ \text{---} \quad \text{---} \end{array} + \dots + \begin{array}{c} \text{---} \quad \text{---} \\ | \quad | \\ \text{---} \quad \text{---} \\ \text{---} \quad \text{---} \end{array} + \dots \right) + \dots
\end{aligned}$$

Figure S2. Normalized exciton basis wavefunctions corresponding to the final states of absorptions in syn-syn **P-T-T-P**. The outer (inner) pairs of horizontal bars correspond to the highest occupied bonding and lowest unoccupied antibonding MOs (HOMOs and LUMOs) of P (T). Not shown are lower energy bonding (higher energy antibonding) MOs that are fully occupied (empty). Electron occupancies of MOs are indicated. Lines and curves connecting MOs are spin-singlet bonds. Ellipses correspond to additional configurations related by mirror-plane and charge-conjugation symmetries.

$$\begin{aligned}
\psi_I: & \left\{ \begin{aligned} & 0.68 \left[\begin{array}{c} \text{---} \text{---} \\ \text{---} \text{---} \\ \text{---} \text{---} \end{array} \right] + 0.55 \left[\begin{array}{c} \text{---} \text{---} \\ \text{---} \text{---} \\ \text{---} \text{---} \end{array} \right] - 0.13 \left[\begin{array}{c} \text{---} \text{---} \\ \text{---} \text{---} \\ \text{---} \text{---} \end{array} \right] + \dots \\ & 0.68 \left[\begin{array}{c} \text{---} \text{---} \\ \text{---} \text{---} \\ \text{---} \text{---} \end{array} \right] - 0.55 \left[\begin{array}{c} \text{---} \text{---} \\ \text{---} \text{---} \\ \text{---} \text{---} \end{array} \right] + 0.13 \left[\begin{array}{c} \text{---} \text{---} \\ \text{---} \text{---} \\ \text{---} \text{---} \end{array} \right] + \dots \end{aligned} \right. \\
\psi_{II}: & \left\{ \begin{aligned} & 0.67 \left[\begin{array}{c} \text{---} \text{---} \\ \text{---} \text{---} \\ \text{---} \text{---} \end{array} \right] - 0.50 \left[\begin{array}{c} \text{---} \text{---} \\ \text{---} \text{---} \\ \text{---} \text{---} \end{array} \right] - 0.13 \left[\begin{array}{c} \text{---} \text{---} \\ \text{---} \text{---} \\ \text{---} \text{---} \end{array} \right] + \dots \\ & 0.67 \left[\begin{array}{c} \text{---} \text{---} \\ \text{---} \text{---} \\ \text{---} \text{---} \end{array} \right] - 0.50 \left[\begin{array}{c} \text{---} \text{---} \\ \text{---} \text{---} \\ \text{---} \text{---} \end{array} \right] - 0.13 \left[\begin{array}{c} \text{---} \text{---} \\ \text{---} \text{---} \\ \text{---} \text{---} \end{array} \right] + \dots \end{aligned} \right. \\
\psi_{III}: & \left\{ \begin{aligned} & 0.40 \left[\begin{array}{c} \text{---} \text{---} \\ \text{---} \text{---} \\ \text{---} \text{---} \end{array} \right] - 0.37 \left[\begin{array}{c} \text{---} \text{---} \\ \text{---} \text{---} \\ \text{---} \text{---} \end{array} \right] + 0.19 \left[\begin{array}{c} \text{---} \text{---} \\ \text{---} \text{---} \\ \text{---} \text{---} \end{array} \right] + \dots \\ & 0.40 \left[\begin{array}{c} \text{---} \text{---} \\ \text{---} \text{---} \\ \text{---} \text{---} \end{array} \right] + 0.37 \left[\begin{array}{c} \text{---} \text{---} \\ \text{---} \text{---} \\ \text{---} \text{---} \end{array} \right] - 0.18 \left[\begin{array}{c} \text{---} \text{---} \\ \text{---} \text{---} \\ \text{---} \text{---} \end{array} \right] + \dots \end{aligned} \right. \\
\psi_{IV}: & 0.53 \left[\begin{array}{c} \text{---} \text{---} \\ \text{---} \text{---} \\ \text{---} \text{---} \end{array} \right] + \dots + 0.17 \left[\begin{array}{c} \text{---} \text{---} \\ \text{---} \text{---} \\ \text{---} \text{---} \end{array} \right] + 0.15 \left[\begin{array}{c} \text{---} \text{---} \\ \text{---} \text{---} \\ \text{---} \text{---} \end{array} \right] + \dots \\
\psi_V: & 0.53 \left[\begin{array}{c} \text{---} \text{---} \\ \text{---} \text{---} \\ \text{---} \text{---} \end{array} \right] - \dots + 0.19 \left[\begin{array}{c} \text{---} \text{---} \\ \text{---} \text{---} \\ \text{---} \text{---} \end{array} \right] - 0.18 \left[\begin{array}{c} \text{---} \text{---} \\ \text{---} \text{---} \\ \text{---} \text{---} \end{array} \right] + \dots
\end{aligned}$$

Figure S3. Normalized exciton basis wavefunctions corresponding to the final states of absorptions in syn-anti **P-T-T-P**. Here first three peaks (I, II, III) are doubly degenerate, hence two eigenstates correspond to these peaks. The outer (inner) pairs of horizontal bars correspond to the highest occupied bonding and lowest unoccupied antibonding MOs (HOMOs and LUMOs) of P (T). Not shown are lower energy bonding (higher energy antibonding) MOs that are fully occupied (empty). Electron occupancies of MOs are indicated. Lines and curves connecting MOs are spin-singlet bonds. Ellipses correspond to additional configurations related by mirror-plane and charge-conjugation symmetries.

IV. CHARGE TRANSFER STATES IN THE GROUND STATE ABSORPTION

Table S2. Calculated energies (in eV), transition dipole couplings with the ground state, and wavefunction characteristics. μ is the transition dipole coupling with the ground state (\AA°). \mathbf{CT}_{CC} , $\mathbf{CT}_{C\beta_1}$, $\mathbf{CT}_{C\beta_2}$, $\mathbf{CT}_{\beta\beta}$, and \mathbf{LE}_β are normalized coefficients of configurations displaying chromophore to chromophore CT, chromophore to nearest bridge CT (and vice versa), chromophore to second nearest bridge CT(vice and versa), bridge to bridge CT and localized excitation on the bridge, respectively.

Connectivity	E	μ	\mathbf{CT}_{CC}	$\mathbf{CT}_{C\beta_1}$	$\mathbf{CT}_{C\beta_2}$	$\mathbf{CT}_{\beta\beta}$	\mathbf{LE}_β
<i>anti-anti</i>	3.21	1.28	0	0.38	0	0	0.11
	3.36	0.97	0	0.14	0	0.54	0
	3.45	0.29	0	0.38	0	0.07	0
	3.52	0.47	0.53	0.08	0.19	0.16	0
<i>syn-syn</i>	3.21	1.43	0	0.38	0	0.14	0
	3.36	0.86	0	0.07	0.11	0.55	0.14
	3.45	0.33	0.10	0.13	0.11	0	0
	3.52	0.21	0.53	0	0.16	0.17	0
<i>syn-anti</i>	3.21	1.27	0	0.08	0.39, 0.37	0	0.13, 0.08
		0.47	0	0.06	0.40, 0.37	0.07	0.09, 0.08
	3.36	0.91	0.11	0.17, 0.15	0.06	0.53	0.14
	3.45	0.30	0.10	0.14	0.20	0.03	0
		0.25	0	0.06	0.23	0.05	0
	3.52	0.27	0.53	0.14, 0.18	0.11, 0.05	0.05	0.05
	3.63	0.22	0	0.43	0.09, 0.08	0	0

V. CHARGE TRANSFER STATES IN THE EXCITED STATE ABSORPTION

Table S3. Calculated energies (in eV), transition dipole couplings with the optical singlet state, and wavefunction characteristics. μ is the transition dipole coupling with the optical singlet state S1. Where \mathbf{CT}_{CC} , $\mathbf{CT}_{C\beta_1}$, $\mathbf{CT}_{C\beta_2}$, $\mathbf{CT}_{\beta\beta}$, and \mathbf{LE}_{β} are normalized coefficients of configurations displaying chromophore to chromophore CT, chromophore to nearest bridge CT (and vice versa), chromophore to second nearest bridge CT (and vice versa), bridge to bridge CT and localized excitation on the bridge, respectively. The complete WFs for the state in *anti-anti-P-T-T-P* at 3.33 eV, in *syn-syn P-T-T-P* at 3.32 eV, and in *syn-anti* at 3.30 eV are dominated by intramonomer HOMO-1 to LUMO/HOMO to LUMO+1 excitation, not charge transfer.

Connectivity	E	μ	\mathbf{CT}_{CC}	$\mathbf{CT}_{C\beta_1}$	$\mathbf{CT}_{C\beta_2}$	$\mathbf{CT}_{\beta\beta}$	\mathbf{LE}_{β}
<i>anti-anti</i>	3.17	2.62	0	0.35	0.06	0	0
	3.33	0.36	0	0	0.13	0.53	0
	3.34	2.21	0	0.19	0	0.11	0
	3.51	0.13	0.53	0.06	0.20	0.14	0
<i>syn-syn</i>	3.17	2.47	0	0.35	0	0.10	0
	3.32	2.07	0	0.09	0.07	0.35	0
	3.37	1.21	0.04	0.07	0.11	0.54	0.14
<i>syn-anti</i>	3.14	2.34	0	0.51	0.09	0.07	0
	3.16	0.17	0	0.51	0.09	0	0
	3.30	2.25	0.06	0.14	0.12, 0.07	0.28	0
	3.34	1.09	0.05	0.19	0.11	0.46	0

**VI. NORMALIZED OVERALL SPIN-SINGLET TRIPLET-TRIPLET
WAVEFUNCTIONS OF SYN-SYN PT2P**

$$\begin{aligned}
 \text{(a)} \quad {}^1(T_{1[P1]}T_{1[P2]}) &= 0.86 \left[\begin{array}{c} \text{Diagram 1} \end{array} \right] + 0.18 \left[\begin{array}{c} \text{Diagram 2} \end{array} \right] + \dots + \dots \\
 \text{(b)} \quad {}^1(T_{1[P1]}T_{1[T1][T2]}) &= \mp 0.56 \left[\begin{array}{c} \text{Diagram 3} \end{array} \right] \pm \dots \pm 0.23 \left[\begin{array}{c} \text{Diagram 4} \end{array} \right] \pm \dots + \dots \\
 \text{(c)} \quad {}^1(T_{1[P1]}T_{1[T2][T1]}) &= -0.56 \left[\begin{array}{c} \text{Diagram 5} \end{array} \right] \pm \dots - 0.23 \left[\begin{array}{c} \text{Diagram 6} \end{array} \right] \pm \dots + \dots \\
 \text{(d)} \quad {}^1(T_{1[T1]}T_{1[T2]}) &= 0.84 \left[\begin{array}{c} \text{Diagram 7} \end{array} \right] + 0.16 \left[\begin{array}{c} \text{Diagram 8} \end{array} \right] + \dots + \dots
 \end{aligned}$$

Figure S4. Normalized wavefunctions of (a) ${}^1(T_{1[P1]}T_{1[P2]})$, (b) ${}^1(T_{1[P1]}T_{1[T1][T2]})$, (c) ${}^1(T_{1[P1]}T_{1[T2][T1]})$ and (d) ${}^1(T_{1[T1]}T_{1[T2]})$ states in *syn-syn-P-T-T-P*.

**VII. NORMALIZED OVERALL SPIN-SINGLET TRIPLET-TRIPLET
WAVEFUNCTIONS OF SYN-ANTI PT2P**

(a)

$${}^1(T_{1[P1]}T_{1[P2]}) = 0.86 \left[\begin{array}{c} \uparrow \downarrow \\ \uparrow \downarrow \\ \uparrow \downarrow \end{array} \right] - 0.18 \left[\begin{array}{c} \uparrow \downarrow \\ \uparrow \downarrow \\ \uparrow \downarrow \end{array} \right] + \dots$$

(b)

$${}^1(T_{1[P1]}T_{1[T1][T2]}) = \left\{ \begin{array}{l} 0.79 \left[\begin{array}{c} \uparrow \downarrow \\ \uparrow \downarrow \\ \uparrow \downarrow \end{array} \right] - 0.33 \left[\begin{array}{c} \uparrow \downarrow \\ \uparrow \downarrow \\ \uparrow \downarrow \end{array} \right] + \dots \\ 0.79 \left[\begin{array}{c} \uparrow \downarrow \\ \uparrow \downarrow \\ \uparrow \downarrow \end{array} \right] - 0.33 \left[\begin{array}{c} \uparrow \downarrow \\ \uparrow \downarrow \\ \uparrow \downarrow \end{array} \right] + \dots \end{array} \right.$$

(c)

$${}^1(T_{1[P1]}T_{1[T2][T1]}) = \left\{ \begin{array}{l} 0.74 \left[\begin{array}{c} \uparrow \downarrow \\ \uparrow \downarrow \\ \uparrow \downarrow \end{array} \right] + 0.31 \left[\begin{array}{c} \uparrow \downarrow \\ \uparrow \downarrow \\ \uparrow \downarrow \end{array} \right] + 0.26 \left[\begin{array}{c} \uparrow \downarrow \\ \uparrow \downarrow \\ \uparrow \downarrow \end{array} \right] + \dots \\ -0.74 \left[\begin{array}{c} \uparrow \downarrow \\ \uparrow \downarrow \\ \uparrow \downarrow \end{array} \right] - 0.31 \left[\begin{array}{c} \uparrow \downarrow \\ \uparrow \downarrow \\ \uparrow \downarrow \end{array} \right] + 0.26 \left[\begin{array}{c} \uparrow \downarrow \\ \uparrow \downarrow \\ \uparrow \downarrow \end{array} \right] + \dots \end{array} \right.$$

(d)

$${}^1(T_{1[T1]}T_{1[T2]}) = 0.84 \left[\begin{array}{c} \uparrow \downarrow \\ \uparrow \downarrow \\ \uparrow \downarrow \end{array} \right] - 0.16 \left[\begin{array}{c} \uparrow \downarrow \\ \uparrow \downarrow \\ \uparrow \downarrow \end{array} \right] + \dots$$

Figure S5. Normalized wavefunctions of (a) ${}^1(T_{1[P1]}T_{1[P2]})$, (b) ${}^1(T_{1[P1]}T_{1[T1][T2]})$, (c) ${}^1(T_{1[P1]}T_{1[T2][T1]})$ and (d) ${}^1(T_{1[T1]}T_{1[T2]})$ states in *syn-anti-P-T-T-P*. Where both (b) and (c) are doubly degenerate triplet-triplet states.

VIII. ENERGY OF TRIPLET-TRIPLET STATES IN SYN-SYN AND SYN-ANTI PT2P

Table S4. Calculated energies (in eV) of various triplet-triplet states for syn-syn and syn-anti
P-T2-P.

State	Energy	
	syn-syn	syn-anti
$^1(\text{T}_{1[P1]}\text{T}_{1[P2]})$	2.08	2.08
$^1(\text{T}_{1[P1]}\text{T}_{1[T1][T2]})$	2.42	2.45
$^1(\text{T}_{1[P1]}\text{T}_{1[T2][T1]})$	2.45	2.47
$^1(\text{T}_{1[T1]}\text{T}_{1[T2]})$	2.77	2.77